Evolution of regenerative Ca-ion wave-packet in Neuronal-firing Fields: Quantum path-integral with serial Shocks

Lester Ingber
Lester Ingber Research
Ashland, Oregon 97520
Email: ingber@alumni.caltech.edu [https://www.ingber.com]

Abstract — *The author previously developed a numerical multivariate path-integral algorithm, PATHINT, which has been applied to several classical physics systems, including statistical mechanics of neocortical interactions, options in financial markets, and other nonlinear systems including chaotic systems. A new quantum version, qPATHINT, has the ability to take into account nonlinear and time-dependent modifications of an evolving system. qPATHINT is shown to be useful to study some aspects of serial changes to systems. Applications ranging from regenerative Ca^{2+} waves in neuroscience to options on blockchains in financial markets are discussed.*
Keywords — *path integral, quantum mechanics, blockchains, parallel code, EEG, vector potential*

I. INTRODUCTION

The author previously developed a numerical multivariate path-integral algorithm, PATHINT. PATHINT has been used for several systems [1][2][3][4][5], The second section briefly describes path integrals and the numerical PATHINT algorithm. A quantum version, qPATHINT, has the ability to take into account nonlinear and serial time-dependent modifications of an evolving system. Quantum computing is here, and in the near future it will be applied to financial products, e.g., blockchains. It not implausible to assume that soon there will be derivatives developed on these products, e.g., options. Then, similar to cases in classical real spaces with PATHINT, qPATHINT is now poised to calculate derivatives in quantum complex spaces. qPATHINT has been successfully baselined to PATHINT. qPATHINT goes beyond simply using quantum computation of derivatives, since the space of the dependent variables themselves may live in quantum worlds [6][7][8][9][10][11]. Another paper has used qPATHINT for options on quantum money [12].

In the second section, qPATHINT is described in the context of the path-integral of a localized wave-packet, propagated as a free particle. A previous paper has described the difficulty in using qPATHINT with an oscillatory system, in the context of comparing generalization of PATHINT to qPATHINT versus the similar generalization of another numerical path-integral algorithm, PATHTREE to qPATHTREE [13][14]. The third section describes a physical-biological problem that arises in neuroscience, in a project undertaken by the author, "Electroencephalographic field influence on calcium momentum waves" [15][16]. This project is the primary motivation to develop qPATHINT. Several studies, fitting EEG data to a model of neocortex that explicitly accounts for multiple scales of neocortical interactions, Statistical Mechanics of Neocortical Interactions (SMNI) [17][18][19][20][1], were performed, modeling Ca^{2+} waves modifying parameterization of background SMNI synaptic parameters. Data was fit to this model using the author's Adaptive Simulated Annealing code [21][22]. qPATHINT is useful to determine the stability of the regenerative process that defines and sustains this specific class of Ca^{2+} waves, wherein reasonable shocks to the waves can occur without seriously damaging its coherence properties. A sub-section considers the application to the study of Free Will.In the fourth section, graphical comparisons are made between the exact and numerical qPATHINT solutions, as a function of different magnetic vector potentials, times of propagation, strengths of serial shocks, and number of off-diagonal elements used in qPATHINT. The Conclusion stresses that these applications of qPATHINT give proofs of concept of these new algorithms and codes.

II. PATH INTEGRALS

The path-integral representation for the short-time propagator P is given in terms of a Lagrangian L by

$$P(S', t' = t + dt \mid S, t) = \frac{1}{2\pi g^2 \Delta t} \exp(-L dt)$$

$$L = \frac{(dS/dt - f)^2}{2g^2}$$

$$\frac{dS}{dt} = \frac{S' - S}{dt} \tag{1}$$

The path integral defines the long-time evolution of P in terms of the action A,

$$P[S(t)]dS(t) = \int \ldots \int DS \exp(-A)$$

$$A = \int_{t_0}^{t} dt' L$$

$$L = \Lambda \Omega^{-1} \int d\vec{S} L$$

$$DS = \prod_{s=1}^{u+1} \prod_{\nu=1}^{\Lambda} (2\pi dt\, g_s^{\nu\,2})^{-1/2} dS_s^{\nu} \delta[S_t = S(t)][\delta[S_0 = S(t_0)] \tag{2}$$

where ν labels the $\vec{S}$-space over the volume Ω, and s labels the $u+1$ time intervals, each of duration dt, spanning $(t - t_0)$. The path integral is a faithful mathematical representation of (properly defined) Fokker-Planck partial differential equations and Langevin stochastic differential equations [23].

2.1 PATHINT

qPATHINT is motivated by a previous non-Monte-Carlo multivariable generalization of a numerical path-integral algorithm [24][25][26], PATHINT, used to develop the long-time evolution of the short-time probability distribution as applied to several studies in chaotic systems [2][5], neuroscience [1][2][4], and financial markets, including two-variable volatility of volatility [3]. These studies suggested applications of some aspects of this algorithm to the standard binomial tree, PATHTREE [14], which is in development for a quantum version, qPATHTREE. Other authors also have applied classical path-integral techniques to options [27]. PATHINT and qPATHINT are particularly well suited to process serial shocks, much more so than other Monte Carlo methods that also are applied to classical and quantum development of probabilities and wave functions [28].

PATHINT develops bins T_{ij} about diagonal terms in the Lagrangian.

$$P_i(t + \Delta t) = T_{ij}(\Delta t)P_j(t)$$

$$T_{ij}(\Delta t) = \frac{2}{\Delta S_{i-1} + \Delta S_i} \int_{S_i - \Delta S_{i-1}/2}^{S_i + \Delta S_i/2} dS \int_{S_j - \Delta S_{j-1}/2}^{S_j + \Delta S_j/2} dS' G(S, S'; \Delta t) \tag{3}$$

T_{ij} is a banded matrix representing the Gaussian nature of the short-time probability centered about the (varying) drift. Fitting data with the short-time probability distribution, effectively using an integral over this epoch, permits the use of coarser meshes than the corresponding stochastic differential equation. The coarser resolution is appropriate, typically required, for numerical solution of the time-dependent path-integral. By considering the contributions to the first and second moments of ΔS^G for small time slices θ, conditions on the time and variable meshes can be derived [24]. The time slice essentially is determined by $\theta \le \overline{L}^{-1}$, where $\overline{L}$ is the "static" Lagrangian with $dS^G / dt = 0$, throughout the ranges of S^G giving the most important contributions to the probability distribution P. The variable mesh, a function of S^G, is optimally chosen such that ΔS^G is measured by the covariance $g^{GG'}$, or $\Delta S^G \approx (g^{GG}\theta)^{1/2}$. PATHINT was generalized by the author to process arbitrary N variable spaces, but in practice only N = 2 was used because of intensive computer resources. The author was Principal Investigator, National Science Foundation (NSF) Pittsburgh Supercomputing Center (PSC) Grant DMS940009P during 1994-1995 on a project, "Porting Adaptive Simulated Annealing and Path Integral Calculations to the Cray; Parallelizing ASA and PATHINT Project (PAPP)". Eight volunteers were selected from many applicants and the PATHINT code was seeded to work on parallel machines. No further work has been done since that time to further develop parallel-coded applications.

2.2 qPATHINT

Similar to the development of qPATHINT described above, the PATHINT C code of about 7500 lines of code was rewritten for the GCC C-compiler to use complex double variables instead of double variables. qPATHINT, using real variables, was baselined to PATHINT by obtaining numerical agreement to previous results using PATHINT to calculate options for financial markets [3]. Note that options calculations include calculations of evolving probability distributions, making such codes very useful for similar calculations in other disciplines. qPATHINT evolves a wave function whose absolute square at any node is a probability, e.g., to determine payoffs at nodes when calculating American options.

_____

2.3 WAVE PACKET EXAMPLE

This example is in one spatial dimension. Note that for the purpose of studying Ca^{2+} ions in the presence of $\mathbf{A}$, the time scales assumed for $\mathbf{A}$ are much larger than the time between regenerative modifications of the ion wave packet. Therefore, during these short times, $\mathbf{A}$ is taken to be constant, time and space independent. In the presence of a magnetic vector potential $\mathbf{A}$ the free particle propagator ψ_F evolves as

$$\psi_F(t) = \int \frac{d\mathbf{p}}{2\pi\hbar} \exp\left[\frac{i}{\hbar}\left(\mathbf{p}(\mathbf{r} - \mathbf{r}_0) - \frac{\mathrm{P}^2 t}{(2m)} \right) \right]$$

$$= \left[\frac{m}{2\pi i\hbar t} \right]^{1/2} \exp\left[\frac{im(\mathbf{r} - \mathbf{r}_0 - q\mathbf{A}t/m)^2}{2\hbar t} - \frac{i(q\mathbf{A})^2 t}{2m\hbar} \right] \tag{4}$$

where the canonical momentum $\mathrm{P} = \mathbf{p} + q\mathbf{A}$. (Note cancellation of $(q\mathbf{A})^2$ terms.) While x also will be used to represent one-dimensional $\mathbf{r}$, three-dimensional notation will be regularly used to emphasize generality to three dimensions. The prefactor would have an exponent of 3/2 instead of 1/2 in three spatial dimensions. This short-time propagator is used here in the numerical qPATHINT code. This also is the result for long times for this particular example, as is verified by standard path-integral calculations [29]. In this paper $\mathbf{A}$ is taken as a constant over the period of several hundred ms, e.g., during highly synchronous neuronal firings during attention tasks, which is a context for one application discussed below. The one-dimensional wave packet ψ starts at $\mathbf{r}$ at $t = 0$, $\mathbf{r}_0$, with momentum $\mathbf{p}_0$ as

$$\psi_0 = \psi(\mathbf{r}_0, t=0) = \left(\frac{1}{\pi\Delta\mathbf{r}^2} \right)^{1/4} \exp\left(-\frac{\mathbf{r}_0^2}{2\Delta\mathbf{r}^2} + i\frac{\mathrm{P}_0 \cdot \mathbf{r}_0}{\hbar} \right) \tag{5}$$

where the initial canonical momentum $\mathrm{P}_0 = \mathbf{p}_0 + q\mathbf{A}_0$. The exact solution for all time for the propagation of the wave packet [29][30] (modified to include $q\mathbf{A}$), ψ_e, is

$$\psi_e(t) = \int d\mathbf{r}_0 \psi_0 \psi_F$$

$$= \left[\frac{1 - i\hbar t/(m\Delta\mathbf{r}^2)}{1 + i\hbar t/(m\Delta\mathbf{r}^2)} \right]^{1/4} \left[\frac{1}{\pi\Delta\mathbf{r}^2 [1 + (\hbar t/(m\Delta\mathbf{r}^2))^2]} \right]^{1/4}$$

$$\exp\left[-\frac{[\mathbf{r} - (\mathrm{P}_0 + q\mathbf{A})t/m]^2}{2\Delta\mathbf{r}^2} \frac{1 - i\hbar t/(m\Delta\mathbf{r}^2)}{1 + (\hbar t/(m\Delta\mathbf{r}^2))^2} + i\frac{\mathrm{P}_0 \cdot \mathbf{r}}{\hbar} - i\frac{(\mathrm{P}_0 + q\mathbf{A})^2 t}{2\hbar m} \right] \tag{6}$$

Since this derivation uses the Stratonovich (standard) calculus, i.e., not the Ito calculus, $\mathbf{A}(t)$ from the free propagator must be evaluated at the midpoint between $\{t - dt, t\}$ [31][23].

2.4 qPATHINT NORMALIZATION

PATHINT and qPATHINT are coded to span any number of offsets from the diagonal kernel/propagator read in as a parameter to the code. qPATHINT reported here normalizes the evolving matrix of distributions according the the square of the evolving wave function $\int d\mathbf{r}\, \psi\psi^*$. The numerical evaluation of the propagator of the wave packet evaluates the propagation of $\psi(\mathbf{r}_0, t=0)$ with multiple small time increments dt of the free propagator $\psi_F(dt)$. The numerical normalization over finite $\int d\mathbf{r}$ will at best only scale the exact propagation as most of the value of ψ is in a finite range only for short times for this wave packet.

III. APPLICATION TO EEG INFLUENCE ON CALCIUM MOMENTUM WAVES

This section gives a summary of the XSEDE project that was developed between February 2013 through June 2016, "Electroencephalographic field influence on calcium momentum waves", which generated interest in developing qPATHTREE and qPATHINT from PATHTREE and PATHINT, resp. This is just one example of studies that may take advantage of these new non-Monte-Carlo algorithms to study sequential development of quantum systems. This review section closely follows other recent papers [13][15].

3.1 FREE WILL

In addition to the intrinsic interest of researching short-term memory (STM) and multiple scales of neocortical interactions via electroencephalography (EEG) data, there is interest in researching possible quantum influences on highly synchronous neuronal firings relevant to STM to understand possible connections to "Free Will" (FW). As pointed out in some recent papers [13][15], if neuroscience ever establishes experimental feedback from quantum-level processes of tripartite synaptic interactions with large-scale synchronous neuronal firings, that are now recognized as being highly correlated with STM and states of attention, then FW may yet be established using the quantum "Free Will Theorem" (FWT) [32][33].

Basically, this means that a Ca^{2+} quantum wave-packet may generate a state proven to have not previously existed. In the context of the basic premise of this paper, this state may be influential in a large-scale pattern of synchronous neuronal firings, thereby rendering this pattern as a truly new pattern not having previously existed. The FWT shows that this pattern, considered as a measurement of the Ca^{2+} quantum wave-packet, surprisingly is correctly identified as itself being a new decision not solely based on previous (deterministic) decisions, even under reasonably stochastic experimental conditions. Only recently has the core SMNI hypothesis since circa 1980 [34][17][18], that highly synchronous patterns of neuronal firings in fact process high-level information, been verified experimentally [35][36]. Clearly, even in the above context, for most people most of the time, internal and external events affecting neural probabilistic patterns of attention give rise to quite practical reasonable FW. However, there also may be some Science that establishes a truly precise FW.

3.2 MOLECULAR PROCESSES CONTRIBUTING TO SYNAPTIC INTERACTIONS

There are many studies on tripartite neuron-astrocyte interactions [37], and on Ca^{2+} waves at tripartite sites. The short summary below is presented to set the context for SMNI calculations of probability distributions of synaptic activity that include background molecular contributions. Several studies have shown that glutamate release from astrocytes through a Ca^{2+}-dependent mechanism can activate receptors located at the presynaptic terminals. Glutamate is the primary neurotransmitter that activates excitatory neuronal firings. Regenerative intercellular calcium waves (ICWs) can travel over 100s of astrocytes, encompassing many neuronal synapses. These ICWs are documented in the control of synaptic activity [38]. Analysis of fluorescence accumulation clearly demonstrates that glutamate is released in a regenerative manner, with subsequent cells that are involved in the calcium wave releasing additional glutamate [39]. Although the full set of mechanisms affecting $[Ca^{2+}]$ and the influences of Ca^{2+} on other mechanism are not yet fully understood and experimentally verified, it is clear that Ca^{2+} waves exist in intercellular and in intracellular media [40]. There are regenerative as well as non-regenerative processes observed, both "locally" at cellular sites as well as into "expanded" regions through which Ca^{2+} travel at relatively fast velocities for large distances over relatively long periods of time [41][15][16].

3.3 INFLUENCE OF SYNCHRONOUS NEURAL FIRINGS

Results of SMNI fits to EEG data give strong confirmation of the SMNI model of STM, and give support to a basic physical mechanism that couples highly synchronous firings to control underlying molecular processes, the canonical momentum $\mathbb{P}$, $\mathbb{P} = \mathbf{p} + q\mathbf{A}$, where $\mathbf{p}$ is the momenta of a Ca^{2+} wave, q the charge of Ca^{2+}, $q = -2e$, e the magnitude of the charge of an electron [15]. Previous papers have used classical physics to calculate and compare the molecular $\mathbf{p}$ and large-scale q $\mathbf{A}$ components of $\mathbb{P}$, demonstrating that indeed they of comparable magnitudes [42][43][16][44]. Also, in the context of quantum mechanics, the wave function of the Ca^{2+}-wave system was calculated, and it was demonstrated that overlap with multiple collisions, due to their regenerative processes, during the observed long durations of hundreds of ms of typical Ca^{2+} waves [41][16] support a Zeno or "bang-bang" effect [45][46][47][48][49][50][51][52] which may promote long coherence times. Of course, the Zeno/"bang-bang" effect may exist only in special contexts, since decoherence among particles is known to be very fast, e.g., faster than phase-damping of macroscopic classical particles colliding with quantum particles [53]. Here, the constant collisions of Ca^{2+} ions as they enter and leave the Ca^{2+} wave packet due to the regenerative process that maintains the wave, may in part shield at least part of the wave, permitting the Zeno/"bang-bang" effect. In any case, qPATHINT as used here provides an opportunity to explore the coherence stability of the wave due to serial shocks of this process.

3.4 CLASSICAL PHYSICS OF $\mathbb{P}$

Previous papers have modeled minicolumns as wires which support neuronal firings, mainly from large neocortical excitatory pyramidal cells in layer V (of six), giving rise to currents which in turn gives rise to electric potentials measured as scalp EEG [42][43][44]. This gives rise to a magnetic vector potential

$$\mathbf{A} = \frac{\mu}{4\pi}\mathbf{I}\log\left(\frac{r}{r_0}\right) \tag{7}$$

which has a log-insensitive dependence on distance. In the brain, $\mu \approx \mu_0$, where μ_0 is the magnetic permeability in vacuum $= 4\pi 10^{-7}$ H/m (Henry/meter), where Henry has units of kg-m-C^{-2}, the conversion factor from electrical to mechanical variables. For oscillatory waves, the magnetic field $\mathbf{B} = \nabla \times \mathbf{A}$ and the electric field $\mathbf{E} = (ic/\omega)\nabla \times \nabla \times \mathbf{A}$ do not have this log dependence on distance. The magnitude of the current is taken from experimental data on dipole moments $\mathbf{Q} = |\mathbf{I}|z$ where $\hat{\mathbf{z}}$ is the direction of the current $\mathbf{I}$ with the dipole spread over z. $\mathbf{Q}$ ranges from 1 pA-m $= 10^{-12}$ A-m for a pyramidal neuron [54], to 10^{-9} A-m for larger neocortical mass [55]. These currents give rise to $q\mathbf{A} \approx 10^{-28}$ kg-m/s. The velocity of a Ca^{2+} wave can be ≈ 20-50 μ m/s. In neocortex, a typical Ca^{2+} wave of 1000 ions, with total mass $m = 6.655 \times 10^{-23}$ kg times a speed of ≈ 20-50 μ m/s, gives $\mathbf{p} \approx 10^{-27}$ kg-m/s. The possibility of magnetism affecting neuronal dynamics is under experimental investigation [56].

3.5   QUANTUM PHYSICS OF $\mathbb{P}$

Previous papers have detailed quantum calculations of the wave function of Ca^{2+} waves in the presence of $\mathbf{A}$ [41][16]. The normalized wave function in momentum space, $\phi(\mathbf{p},t)$, is

$$\phi(\mathbf{p},0) = (2\pi(\Delta\mathbf{p})^2)^{-3/4} \exp\left[-\frac{(\mathbf{p}-\mathbb{P}_0)^2}{4(\Delta\mathbf{p})^2}\right]$$

$$U(\mathbf{p},t) = \exp\left[i\frac{(\mathbf{p}+q\mathbf{A})^2 t}{2m\hbar}\right]$$

$$\phi(\mathbf{p},t) = \phi(\mathbf{p},0)U(\mathbf{p},t) \tag{8}$$

where again $\mathbb{P}_0 = \mathbf{p}_0 + q\mathbf{A}_0$. Estimates in this sub-section take $\mathbb{P}_0 \approx \mathbf{p}_0$.

In momentum space the wave packet, consider $\phi(\mathbf{p},t)$ being "kicked" from $\mathbf{p}$ to $\mathbf{p}+\delta\mathbf{p}$, and simply assume that random repeated kicks of $\delta\mathbf{p}$ result in $<\delta\mathbf{p}>\approx 0$, and each kick keeps the variance $\Delta(\mathbf{p}+\delta\mathbf{p})^2 \approx \Delta(\mathbf{p})^2$. Then, the overlap integral at the moment t of a typical kick between the new and old state is

$$<\phi^*(\mathbf{p}+\delta\mathbf{p},t)\,|\,\phi(\mathbf{p},t)>=$$

$$\exp\left[\frac{i8\delta\mathbf{p}\Delta\mathbf{p}^2\hbar m(q\mathbf{A}+\mathbb{P}_0)t - 4(\delta\mathbf{p}\Delta\mathbf{p}^2 t)^2 + -(\delta\mathbf{p}\hbar m)^2}{8(\Delta\mathbf{p}\hbar m)^2}\right] \tag{9}$$

where $\phi(\mathbf{p}+\delta\mathbf{p},t)$ is the normalized wave function in $\mathbf{p}+\delta\mathbf{p}$ momentum space. A crude estimate is obtained of the survival time $A(t)$ and survival probability $p(t)$ [46],

$$A(t) = <\phi^*(\mathbf{p}+\delta\mathbf{p},t)\,|\,\phi(\mathbf{p},t)>$$

$$p(t) = |A(t)|^2 \tag{10}$$

These numbers yield:

$$<\phi^*(\mathbf{p}+\delta\mathbf{p},t)\,|\,\phi(\mathbf{p},t)>= \exp\left[i(1.67\times10^{-1}t - 1.15\times10^{-2}t^2) - 1.25\times10^{-7}\right] \tag{11}$$

Even many small repeated kicks do not appreciably affect the real part of ϕ, and these projections do not appreciably destroy the original wave packet, giving a survival probability per kick as $p(t) \approx \exp(-2.5\times10^{-7}) \approx 1 - 2.5\times10^{-7}$. Both time-dependent phase terms in the exponent are sensitive to time scales on the order of 1/10 s, scales prominent in STM and in synchronous neural firings measured by EEG. This suggests that $\mathbf{A}$ effects on Ca^{2+} wave functions may maximize their influence on STM at frequencies consistent with synchronous EEG during STM by some mechanisms not yet determined.

3.6   COHERENCE OF REGENERATIVE PROCESSES

The short summary above argues for Zeno-type long-time coherence of Ca^{2+} wave packets, during which they are affected by the $\mathbb{P} = \mathbf{p} + q\mathbf{A}$ interaction due to highly synchronous neural activity, and in turn their role in modifying synaptic interactions is affected. This study using qPATHINT is motivated to further calculate just how much shock the Ca^{2+} wave packets may endure by virtue of the regenerative process that defines it.

VI.   SERIAL SHOCKS

This path-integral study is used to examine the nature of disturbances on the propagation of ψ due to time-dependent serial shocks in the mass as a proxy for changing momenta due to the regenerative process described above, wherein Ca^{2+} ions aperiodically leave or join the wave packet. This example uses qPATHINT to numerically study the propagation of the wave packet and compare it to exact solution. The time and space variables are determined independently with this algorithm. The range of space variables was taken to be $[-10^{-5}, 10^5]$ m. As mentioned above, the space mesh is best determined by the square root of the product of the diffusion times dt of the free particle, which is 4×10^{-8} s, yielding a diagonal mesh of 500 points, and a matrix of approximately 500 times the off-diagonal (od) spread. A few points at the ends of the diagonal are of course not used. This description is for the half-spread from the diagonal, so well over 10,000 points can be used in the kernel for cases considered here. The time mesh is best taken by sampling the Lagrangian of the free particle, in turn dependent on the space mesh in this case, which is about 10^{-3}. Therefore, $dt = 10^{-3}$ and 4×10^{-8} were used in these calculations, yielding 100 foldings of the propagator every 0.1 s of time. The standard C-code uniform integer random number generator, rand(), is scaled to develop random real numbers within [-1,1], which is multiplied by mass of 1000 Ca^{2+} ions, multiplied by a "shock" multiplier η, each time the function ψ_F is called. Shapes of the distribution are generally retained for all shocks relative to no shocks with parameter $\eta = 0$, with more disruptions at higher shocks and longer propagation.

_____

4.1 GRAPHICAL RESULTS

Graphs are developed using data for real (Rl) and imaginary (Im) parts of the numerical path-integral evolution of ψ and of the exact ψ_e wave functions. In each figure, the title

$$\psi(qA = W, t = X, \eta = Y, od = Z) \tag{12}$$

is used to denote each such set of 4 graphs, where

$$W = \{0, 10^{-28}, 10^{-26}\}$$
$$X = \{0.5, 0.1, 0.15, 2.0\}$$
$$Y = \{0, 0.01, 0.1, 0.2\}$$
$$Z = \{3, 7, 9, 13\} \tag{13}$$

The file https://www.ingber.com/path17_quantum_pathint_shocks_supp.pdf contains all 192 cases of such figures, each figure containing 4 such graphs. Fig. 1 gives graphical results for qPATHINT calculations compared to exact solutions, for $qA = 10^{-28}$, $t = 0.15$, $\eta = 0$, and $od = 13$. Note how the presence of finite qA adds additional structure to the wave packet.
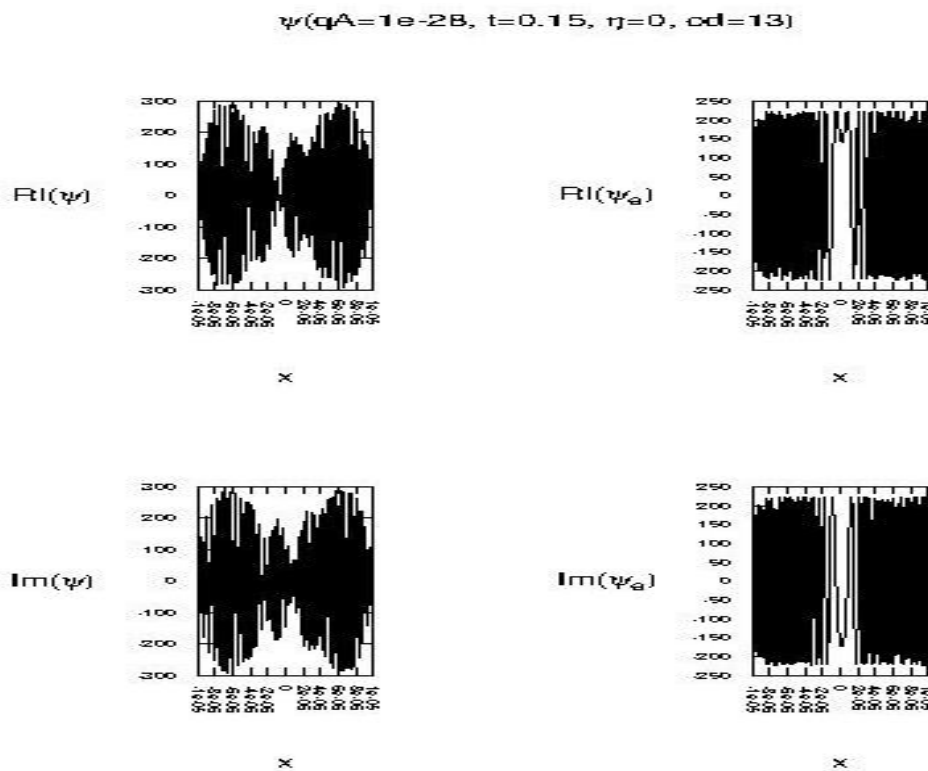

FIG. 1. ψ *with* $qA = 10^{-28}$, $t = 0.15$, $\eta = 0$, *and* $od = 13$.

Fig. 2 gives graphical results for qPATHINT calculations compared to exact solutions, for $qA = 10^{-28}$, $t = 0.15$, $\eta = 0.1$, and $od = 13$. Note how shocks in the presence of finite qA disrupts the wave packet.
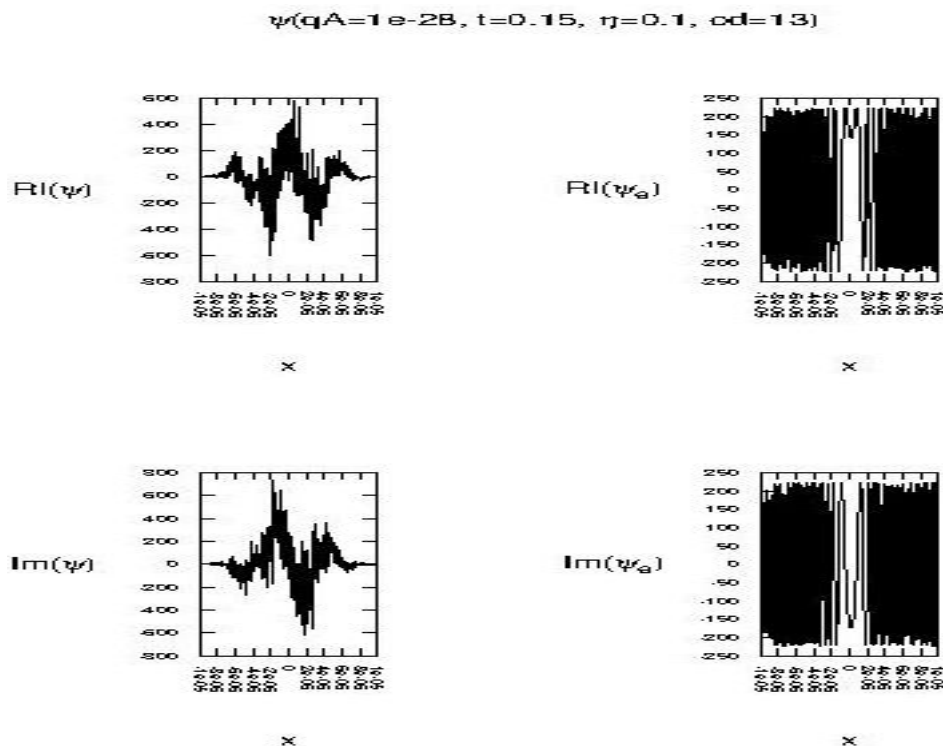
$\psi(qA=1e\text{-}2B, t=0.15, \eta=0.1, od=13)$

FIG. 2. ψ *with* $qA = 10^{-28}$, $t = 0.15$, $\eta = 0.1$, *and* $od = 13$.

V. CONCLUSION

A numerical path-integral algorithm, PATHINT, has been generalized to complex variable spaces, resulting in a new qPATHINT code useful for quantum wave functions and/or quantum probability functions. PATHINT has already applied to various systems, including financial-market options, chaotic studies, and neuroscience. Similar to PATHINT, qPATHINT's accuracy is best for moderate-noise systems. Much CPU in qPATHINT is used just calculating the distribution at all nodes. The added generalization of dealing with N dimensions in qPATHINT requires a lot of overhead taking care of indices and boundaries within many for-loops. Parallel processing makes these codes more efficient in real-time. qPATHINT is applied to a free wave packet, and it handles oscillatory system reasonably well. However, of course this system has an infinite domain, and so calculations performed here cannot be accurate given the finite ranges used. However, a proof of principle has been demonstrated, which is poised to handle quantum options on quantum systems, in finance and in blockchains. qPATHINT can be useful in multiple disciplines, e.g., neuroscience and financial markets. A neuroscience example is given here. A proper treatment of financial options often requires inclusion of aperiodic dividends and distributions that deviate nonlinearly from Gaussian of log-normal [3][14].

REFERENCES

[1]. L. Ingber. Statistical mechanics of neocortical interactions: Path-integral evolution of short-term memory. Physical Review E, 49(5B):4652–4664, 1994. https://www.ingber.com/smni94_stm.pdf.

[2]. L. Ingber. Path-integral evolution of multivariate systems with moderate noise. Physical Review E, 51(2):1616–1619, 1995. https://www.ingber.com/path95_nonl.pdf.

[3]. L. Ingber. High-resolution path-integral development of financial options. Physica A, 283(3-4):529–558, 2000. https://www.ingber.com/markets00_highres.pdf.

[4]. L. Ingber and P.L. Nunez. Statistical mechanics of neocortical interactions: High resolution path-integral calculation of short-term memory. Physical Review E, 51(5):5074–5083, 1995. https://www.ingber.com/smni95_stm.pdf.

[5]. L. Ingber, R. Srinivasan, and P.L. Nunez. Path-integral evolution of chaos embedded in noise: Duffing neocortical analog. Mathematical Computer Modelling, 23(3):43–53, 1996. https://www.ingber.com/path96_duffing.pdf.

[6]. S. Aaronson and P. Christiano.Quantum money from hidden subspaces.Technical Report arXiv:1203.4740 [quant-ph], MIT, Cambridge, MA, 2012.

_____

[7]. L. Accardi and A. Boukas. The quantum black-scholes equation. Technical Report arXiv:0706.1300 [q-fin.PR], U di Roma Torvergata, Rome, 2007.

[8]. B.E. Baaquie, C. Coriano, and M. Srikant. Quantum mechanics, path integrals and option pricing: Reducing the complexity of finance. Technical Report arXiv:cond-mat/0208191 [cond-mat.soft], National U Singapore, Singapore, 2002.

[9]. J. Jogenfors. Quantum bitcoin: An anonymous and distributed currency secured by the no-cloning theorem of quantum mechanics. Technical Report arXiv:1604.01383 [quant-ph], Linkoping U, Linkoping, Sweden, 2016.

[10]. K. Meyer. Extending and simulating the quantum binomial options pricing model. Technical Report Thesis, U Manitoba, Winnipeg, Canada, 2009. http://hdl.handle.net/1993/3154.

[11]. E.W. Piotrowski, M. Schroeder, and A. Zambrzycka. Quantum extension of european option pricing based on the ornstein-uhlenbeck process. Physica A, 368(1):176–182, 2005.

[12]. L. Ingber. Options on quantum money:: Quantum path-integral with serial shocks. International Journal of Innovative Research in Information Security, 4(2):7–13, 2017. http://dx.doi.org/10.17632/jvpmpmfhfs.1.

[13]. L. Ingber. Path-integral quantum PATHTREE and PATHINT algorithms. International Journal of Innovative Research in Information Security, 3(5):1–15, 2016a. http://dx.doi.org/10.17632/xspkr8rvks.1.

[14]. L. Ingber, C. Chen, R.P. Mondescu, D. Muzzall, and M. Renedo. Probability tree algorithm for general diffusion processes. Physical Review E, 64(5):056702–056707, 2001. https://www.ingber.com/path01_pathtree.pdf.

[15]. L. Ingber. Statistical mechanics of neocortical interactions: Large-scale EEG influences on molecular processes. Journal of Theoretical Biology, 395:144–152, 2016b. http://dx.doi.org/10.1016/j.jtbi.2016.02.003.

[16]. L. Ingber, M. Pappalepore, and R.R. Stesiak. Electroencephalographic field influence on calcium momentum waves. Journal of Theoretical Biology, 343:138–153, 2014. http://dx.doi.org/10.1016/j.jtbi.2013.11.002.

[17]. L. Ingber. Statistical mechanics of neocortical interactions. i. basic formulation. Physica D, 5:83–107, 1982. https://www.ingber.com/smni82_basic.pdf.

[18]. L. Ingber. Statistical mechanics of neocortical interactions. dynamics of synaptic modification. Physical Review A, 28:395–416, 1983. https://www.ingber.com/smni83_dynamics.pdf.

[19]. L. Ingber. Statistical mechanics of neocortical interactions. derivation of short-term-memory capacity. Physical Review A, 29:3346–3358, 1984. https://www.ingber.com/smni84_stm.pdf.

[20]. L. Ingber. Statistical mechanics of neocortical interactions: Stability and duration of the 7+-2 rule of short-term-memory capacity. Physical Review A, 31:1183–1186, 1985. https://www.ingber.com/smni85_stm.pdf.

[21]. L. Ingber. Adaptive simulated annealing (ASA). Technical Report Global optimization C-code, Caltech Alumni Association, Pasadena, CA, 1993. https://www.ingber.com/#ASA-CODE.

[22]. L. Ingber. Adaptive simulated annealing. In Jr. H.A. Oliveira, A. Petraglia, L. Ingber, M.A.S. Machado, and M.R. Petraglia, editors, Stochastic global optimization and its applications with fuzzy adaptive simulated annealing, pages 33–61. Springer, New York, 2012a. Invited Paper. https://www.ingber.com/asa11_options.pdf.

[23]. F. Langouche, D. Roekaerts, and E. Tirapegui. Discretization problems of functional integrals in phase space. Physical Review D, 20:419–432, 1979.

[24]. M.F. Wehner and W.G. Wolfer. Numerical evaluation of path-integral solutions to fokker-planck equations. I. Physical Review A, 27:2663–2670, 1983a.

[25]. M.F. Wehner and W.G. Wolfer. Numerical evaluation of path-integral solutions to fokker-planck equations. II. restricted stochastic processes. Physical Review A, 28:3003–3011, 1983b.

[26]. M.F. Wehner and W.G. Wolfer. Numerical evaluation of path integral solutions to fokker-planck equations. III. time and functionally dependent coefficients. Physical Review A, 35:1795–1801, 1987.

[27]. B. Balaji. Option pricing formulas and nonlinear filtering: a feynman path integral perspective. Signal Processing, Sensor Fusion, and Target Recognition XXII, 8745:1–10, 2013. http://dx.doi.org/10.1117/12.2017901.

[28]. G.P. Lepage. Lattice QCD for novices. Technical Report arXiv:hep-lat/0506036, Cornell, Ithaca, NY, 2005.

[29]. K. Schulten. Quantum mechanics. Technical Report Lecture Notes, U. Illinois, Urbana, IL, 1999. http://www.ks.uiuc.edu/Services/Class/PHYS480/.

[30]. B. Simons. Advanced quantum mechanics. Technical Report Lecture Notes, U. Cambridge, Cambridge UK, 2009. http://www.tcm.phy.cam.ac.uk/ bds10/aqp/handout_charged.pdf.

[31]. B. Gaveau, E. Mihokova, M. Roncadelli, and L.S. Schulman. Path integral in a magnetic field using the trotter product formula. American Journal of Physics, 72:385–388, 2004.

[32]. J. Conway and S. Kochen. The free will theorem. Technical Report arXiv:quant-ph/0604079 [quant-ph], Princeton U, Princeton, NJ, 2006.

[33]. J. Conway and S. Kochen. The strong free will theorem. Notices of the American Mathematical Society, 56(2):226–232, 2009.

[34]. L. Ingber. Towards a unified brain theory. Journal Social Biological Structures, 4:211–224, 1981. https://www.ingber.com/smni81_unified.pdf.

[35]. J. Asher. Brain's code for visual working memory deciphered in monkeys NIH-funded study. Technical Report NIH Press Release, NIH, Bethesda, MD, 2012.

_____

http://www.nimh.nih.gov/news/science-news/2012/in-sync-brain-waves-hold-memory-of-objects-just-seen.shtml.

[36]. R.F. Salazar, N.M. Dotson, S.L. Bressler, and C.M. Gray. Content-specific fronto-parietal synchronization during visual working memory. Science, 338(6110):1097–1100, 2012. http://dx.doi.org/10.1126/science.1224000.

[37]. A. Pereira and F.A. Furlan. On the role of synchrony for neuron-astrocyte interactions and perceptual conscious processing. Journal of Biological Physics, 35(4):465–480, 2009.

[38]. E. Scemes and C. Giaume. Astrocyte calcium waves: What they are and what they do. Glia, 54(7):716–725, 2006. http://dx.doi.org/10.1002/glia.20374.

[39]. B. Innocenti, V. Parpura, and P.G. Haydon. Imaging extracellular waves of glutamate during calcium signaling in cultured astrocytes. Journal of Neuroscience, 20(5):1800–1808, 2000.

[40]. W.N. Ross. Understanding calcium waves and sparks in central neurons. Nature Reviews Neuroscience, 13:157–168, 2012.

[41]. L. Ingber. Calculating consciousness correlates at multiple scales of neocortical interactions. In A. Costa and E. Villalba, editors, Horizons in Neuroscience Research, pages 153–186. Nova, Hauppauge, NY, 2015. ISBN: 978-1-63482-632-7. Invited paper. https://www.ingber.com/smni15_calc_conscious.pdf.

[42]. L. Ingber. Computational algorithms derived from multiple scales of neocortical processing. In A. Pereira, E. Massad, and N. Bobbitt, editors, Pointing at Boundaries: Integrating Computation and Cognition on Biological Grounds, pages 1–13. Springer, New York, 2011. Invited Paper. http://dx.doi.org/10.1007/s12559-011-9105-4.

[43]. L. Ingber. Columnar EEG magnetic influences on molecular development of short-term memory. In G. Kalivas and S.F. Petralia, editors, Short-Term Memory: New Research, pages 37–72. Nova, Hauppauge, NY, 2012b. Invited Paper. https://www.ingber.com/smni11_stm_scales.pdf.

[44]. P.L. Nunez, R. Srinivasan, and L. Ingber. Theoretical and experimental electrophysiology in human neocortex: Multiscale correlates of conscious experience. In M.M. Pesenson, editor, Multiscale Analysis and Nonlinear Dynamics: From genes to the brain, pages 149–178. Wiley, New York, 2013. http://dx.doi.org/10.1002/9783527671632.ch06.

[45]. P. Facchi, D.A. Lidar, and S. Pascazio. Unification of dynamical decoupling and the quantum zeno effect. Physical Review A, 69(032314):1–6, 2004.

[46]. P. Facchi and S. Pascazio. Quantum zeno dynamics: mathematical and physical aspects. Journal of Physics A, 41(493001):1–45, 2008.

[47]. G. Giacosa and G. Pagliara. Quantum zeno effect by general measurements. Physical Review A, 052107:1–5, 2014.

[48]. W. Kozlowski, S.F. Caballero-Benitez, and I.B. Mekhov. Non-hermitian dynamics in the quantum zeno limit. Technical Report arXiv:1510.04857 [quant-ph], U Oxford, Oxford, UK, 2015.

[49]. M.M. Muller, S. Gherardini, and F. Caruso. Quantum zeno dynamics through stochastic protocols. Technical Report arXiv:1607.08871v1 [quant-ph], U Florence, Florence, Italy, 2016.

[50]. Y.S. Patil, S. Chakram, and M. Vengalattore. Measurement-induced localization of an ultracold lattice gas. Physical Review Letters, 115(140402):1–5, 2015. http://link.aps.org/doi/10.1103/PhysRevLett.115.140402.

[51]. S.L. Wu, L.C. Wang, and X.X. Yi. Time-dependent decoherence-free subspace. Journal of Physics A, 405305:1–11, 2012.

[52]. P. Zhang, Q. Ai, Y. Li, D. Xu, and C. Sun. Dynamics of quantum zeno and anti-zeno effects in an open system. Science China Physics, Mechanics and Astronomy, 57(2):194–207, 2014. http://dx.doi.org/10.1007/s11433-013-5377-x.

[53]. J. Preskill. Quantum mechanics. Technical Report Lecture Notes, Caltech, Pasadena, CA, 2015. http://www.theory.caltech.edu/people/preskill/ph219/.

[54]. S.Murakami and Y. Okada. Contributions of principal neocortical neurons to magnetoencephalography and electroencephalography signals. Journal of Physiology, 575(3):925–936, 2006.

[55]. P.L. Nunez and R. Srinivasan. Electric Fields of the Brain: The Neurophysics of EEG, 2nd Ed. Oxford University Press, London, 2006.

[56]. M.A. Wheeler, C.J. Smith, M. Ottolini, B.S. Barker, A.M. Purohit, R.M. Grippo, R.P. Gaykema, A.J. Spano, M.P. Beenhakker, S. Kucenas, M.K. Patel, C.D. Deppmann, and A.D. Guler. Genetically targeted magnetic control of the nervous system. Nature Neuroscience, 19:756–761, 2016. http://dx.doi.org/10.1038/nn.4265.